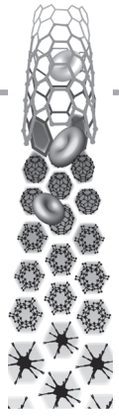

Advances in localized surface plasmon resonance spectroscopy biosensing

In recent years, localized surface plasmon resonance (LSPR) spectroscopy advancements have made it a sensitive, flexible tool for probing biological interactions. Here, we describe the basic principles of this nanoparticle-based sensing technique, the ways nanoparticles can be tailored to optimize sensing, and examples of novel LSPR spectroscopy applications. These include detecting small molecules via protein conformational changes and resonance LSPR spectroscopy, as well as coupling LSPR with mass spectrometry to identify bound analytes. The last few sections highlight the advantages of single nanoparticle LSPR, in that it lowers limits of detection, allows multiplexing on the nanometer scale, and enables free diffusion of sensors in solution. The cases discussed herein illustrate creative ways that LSPR spectroscopy has been improved to achieve new sensing capabilities.

KEYWORDS: biosensing ■ imaging ■ LSPR ■ multiplex ■ nanoparticle ■ tracking

Laura B Sagle[1], Laura K Ruvuna[1], Julia A Ruemmele[1] & Richard P Van Duyne[†1]

[1]Northwestern University, Department of Chemistry, 2145 Sheridan Road, Evanston, IL 60208-3113 USA
[†]Author for correspondence:
Tel.: +1 847 492 3516
Fax: +1 847 491 7713
vanduyne@chem.northwestern.edu

Biosensing has traditionally employed spectroscopic techniques that measure biological interactions in solution [1–5]; however, performing assays on a surface has certain advantages: surface assays require less sample than solution assays [6]; they permit real-time measurements [7]; they are readily amenable to high-throughput sensing since probe functionalized surfaces are easily washed and regenerated enabling sequential measurements [8–10]; and a single surface can be functionalized with an assortment of probes for multiplexed simultaneous sensing [11,12]. One of the most common biological assays is ELISA, in which an unknown protein or antigen is bound to the surface and detected via its interaction with an antibody that is labeled to an enzyme to produce a detectable signal [13,14]. This method has been used to detect analytes at attomolar concentrations using new labeling schemes [15]. One major limitation is the need for a labeled, enzyme-linked antibody that is capable of binding to the protein of interest with high affinity. Surface plasmon resonance (SPR) spectroscopy is one method that has gained popularity to measure biomolecular interactions without the need for labels [16–19]. This technique senses the refractive index (RI) of the environment near a planar noble metal surface by measuring the parameters of light (angle and wavelength), which excite surface plasmons at the noble metal surface. SPR has been used to detect analytes down to the femtomolar range [19]. For the most part SPR and localized surface plasmon resonance (LSPR) have similar advantages and limitations; however, the long field decay length (greater than 100 nm) makes the measurement prone to interference from changes in the bulk RI, such as those caused by temperature fluctuations [20]. Furthermore, measuring protein conformational changes and small ligand binding is often confined to proteins within a matrix, which can drastically affect kinetics [21,22]. Another commonly used label-free biosensing technique is quartz crystal microbalance, in which the binding of a biological analyte is detected as a change in frequency of a quartz crystal resonator. This technique, especially when combined with electrochemistry, has been shown to be quite sensitive and can detect submonolayer coverage (nanomolar range) of biological analytes [23,24]. Finally, it has been shown that label-free sensing can reach limits of detection that are comparable with ELISA using field-effect transistors and have detected biomolecules in the attomolar concentration range [25–27]. These devices, typically made from silicon nanowires, undergo changes in resistivity upon analyte binding to the surface. Unfortunately, this type of device often requires difficult and expensive fabrication processes.

The major drawback of these label-free techniques is that they either require expensive instrumentation, or sensor fabrication is difficult and expensive. LSPR spectroscopy offers easy sensor fabrication and inexpensive instrumentation while retaining all the advantages characteristic of label-free surface sensing, in some cases even demonstrating improved capabilities over other techniques. For example, the

future medicine part of fsg

considerably shorter field decay length for LSPR (5–6 nm) over SPR (100 nm) makes LSPR less sensitive to interference from solution RI fluctuations, but more sensitive to changes on the surface. LSPR sensors are primarily noble metal nanoparticles, which can be functionalized individually to bind a variety of analytes, making it optimal for miniaturized, multiplexed sensing (Figure 1) [28,29]. Single nanoparticle (SNP) LSPR-based biosensing is expected to yield greater sensitivity than the techniques mentioned above, and currently, the mass detection limits have been pushed down to the zeptomole range [30,31]. Although LSPR sensors typically comprise nanoparticle arrays attached to solid supports, SNP LSPR can be performed on nanoparticles moving freely in solution. Tracking nanoparticle motion provides an additional signature for monitoring binding events. This versatility in signal transduction platforms is one major advantage of LSPR-based biosensing techniques.

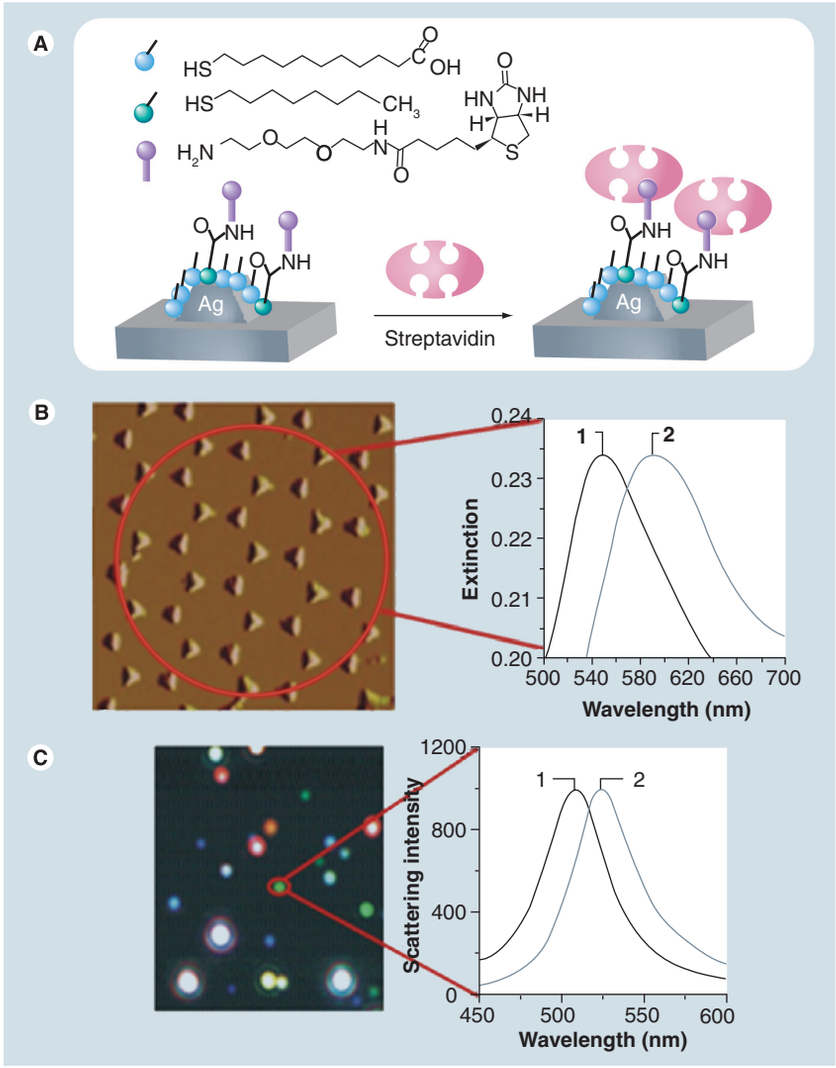

Figure 1. Two different methods for localized surface plasmon resonance sensing streptavidin binding to biotin. (A) The reaction on a periodic particle array fabricated using nanosphere lithography. **(B)** An atomic force microscopy image of a periodic particle array and, to the right, the localized surface plasmon resonance spectra before (1) and after (2) strepatvidin binding [31]. **(C)** A representative darkfield image of many individual Ag nanoparticles. The scattering spectra of a single nanoparticle before (1) and after (2) streptavidin binding.
Reproduced with permission from [33].

Localized surface plasmon resonance biosensors consist of three major components: a plasmonic surface for signal transduction; a passivating layer to minimize nonspecific binding and for optional probe attachment; and a probe layer for specific target recognition. Figure 1 shows LSPR data from two different LSPR sensors that have the same active probe layer, biotin, and hence detect the same analyte, streptavidin. Figure 1A & 1B shows a schematic, atomic force microscopy image, and streptavidin response for a nanoparticle array fabricated on a glass slide by nanosphere lithography [32–34]. The extinction spectra are ensemble measurements of many nanoparticles within the focal spot of the UV-Vis spectrometer. Figure 1C shows a scattered light image of SNPs fixed to a surface and the streptavidin response of one representative nanoparticle; in this case each spectrum is the scattering from a SNP [35]. The spectral maxima shift of the two sensors have similar magnitudes, approximately 25 nm, demonstrating that a SNP is as effective as nanoparticle arrays. Other platforms have been developed that involve either coupling plasmonic particles to both the probe and analyte or to both ends of the same biological molecule, such as DNA. As the probe and analyte bind or the DNA molecules bend, the plasmonic particles come into close proximity, resulting in plasmonic coupling. This produces very large shifts in the LSPR spectrum, which are typically much larger than those observed from changes in RI [36–39].

In this article, we outline the fundamentals of plasmonic sensing as well as highlight a number of new LSPR sensing modalities developed in the past 5 years. The 'LSPR fundamentals' and 'Correlated physical and optical properties of nanoparticles' sections provide a basic explanation of LSPR spectroscopy, how it can be used for biosensing, and the parameters that determine the sensing properties of an LSPR sensor. The 'Detecting small analytes via protein conformational changes' section through to the 'Combined MS & LSPR' section discuss specific examples where LSPR capabilities have been expanded beyond sensing protein binding to measure protein conformational changes, small

molecule binding and to definitively identify bound analytes. Finally, the 'SNP LSPR' section through to the 'Multiplexed biological imaging using LSPR' section describe the capabilities that are unique to SNP LSPR sensing.

LSPR fundamentals

The optical properties of nanoparticles have been observed since circa 400 AD when the Lycurgus Cup was created [40]. This vessel comprises gold nanoparticles, which cause it to appear green when light is reflected from the surface but appear bright red when light passes through the cup. This is due to excitation of the localized surface plasmons on the nanoparticles and only occurs in materials with large, negative real and small, positive imaginary dielectric constants. In the last 20 years, great strides have been made towards understanding this phenomenon. The optical, or plasmonic, properties of nanoparticles have been exploited for a wide range of applications from label-free biochemical sensors [41,42], to optical waveguides and switches [43,44], to surface-enhanced and tip-enhanced Raman spectroscopy [45,46], and to subwavelength imaging and lithography [47,48].

When light impinges upon a nanoparticle with a diameter that is smaller than the wavelength of light, it causes a collective oscillation of the conduction electrons at a frequency known as the LSPR [49,50]. The extinction spectrum as a function of wavelength displays a peak at the LSPR frequency, which is due to absorption and scattering of the light by the nanoparticles [51–53]. This can be calculated according to Mie theory, EQUATION 1:

$$E(\lambda)\frac{(1+\chi)^2 8\pi^2 \mathrm{Na}^3 \varepsilon_E^{3/2}}{3\lambda \ln(10)}\left[\frac{\varepsilon_i}{(\varepsilon_r+\chi\varepsilon_E)^2+\varepsilon_i^2}\right] \quad (1)$$

where N is the number of particles in the sensing area, a is the radius of the particles, χ is a factor correlated with nanoparticle shape, ε_E is the dielectric constant of the external medium, and ε_r and ε_i are the real and imaginary components of the metal dielectric function, respectively [54,55]. It is important to note that χ in this expression has only been solved analytically for spherical particles, and must be approximated for all other shapes [56]. The dielectric constant and RI of the external medium are directly related via:

$$\varepsilon_E = n_E^2 \quad (2)$$

The size, shape and metal (which dictates the dielectric constants) of the nanoparticle, can be varied to tune the LSPR spectrum as described in the 'Multiplexed biological imaging using LSPR' section. A change in ε_E or RI, n_E, shifts the spectral peak position and serves as the basis for biosensing [57–59]. When a biological molecule binds to the nanoparticle, it displaces the solvent and increases the effective ε_E (or n_E) around the nanoparticle, shifting in the extinction peak to longer wavelengths.

The RI of a typical protein is approximately 1.45, but the extent that a protein layer shifts the λ_{max} depends on its protein packing density. The shift ($\Delta\lambda_{max}$) is expressed by EQUATION 3,

$$\Delta\lambda_{max} = m(n_A - n_E)(1 - exp(-2d/l_d)) \quad (3)$$

where m is the RI sensitivity and is often referred to as the m-value, (n_A-n_E) is the RI difference between the biomolecular analyte (n_A) and the bulk solvent environment (n_E), d is the optical thickness of the protein layer coating the nanoparticles, and l_d is the electromagnetic field decay length [33,60]. Thus, from a given LSPR response, it is possible to calculate the optical thickness of the layer, which can be converted to a quantitative coverage of biological molecules on the nanoparticle surface. This is beneficial when designing probe surface coatings to maximize the signal for analyte capture. LSPR can be used to determine binding constants and rate constants by plotting $\Delta\lambda_{max}$ as a function of analyte concentration or time, respectively [33,60].

Correlated physical & optical properties of nanoparticles

The ultimate biosensing goal is to generate the maximum signal for the lowest concentration of analyte. The size, shape and metal of a nanoparticle affect the extinction spectrum and hence its refractive index sensitivity to the environment. These physical properties can be tuned to attain the optimal LSPR signal for any reaction of interest. As discussed in the 'Resonance-enhanced LSPR' section, the sensitivity of the LSPR peak position to the external RI has been extensively studied; however, correlating the physical properties of a particle with its spectrum has only recently been carried out at the single particle level [61]. These correlations must be made on the single particle level, as nanoparticle samples are both structurally and optically heterogeneous. Hence, ensemble measurements do not have the necessary resolution to draw detailed correlations between the physical and optical properties of nanoparticles. Using dark field microscopy, which measures scattered light from individual nanoparticles, Sherry *et al.*

compared single particle LSPR scattering spectra with the ensemble extinction spectrum for Ag nanoprisms (FIGURE 2A) [62]. The λ_{max} of four randomly chosen individual particles were close to the ensemble λ_{max}, but the variation in the single particle spectra demonstrate the particle-to-particle heterogeneity within this sample. Furthermore, the single particle spectra can be modeled using the discrete dipole approximation and FIGURE 2B demonstrates that experimental data can be well described by theory [62]. These combined results show that an ensemble spectrum comprises many unique single particle spectra, and, therefore, precise correlations between spectral and physical properties require single particle measurements. The following paragraphs describe how the nanoparticle material, size and shape affect their LSPR sensing capabilities.

There are many types of metal nanoparticles that can support plasmons (Pd, [63] Pt, [64] Al, [65], Au and Ag); however, gold and silver nanoparticles are the most common, and, therefore, are the focus of this article. Silver nanoparticles have a greater m-value than gold nanoparticles of the same size and shape, 161 nm/RIU versus 44 nm/RIU for silver and gold, respectively [66,67]. This is due to the differences in the real and imaginary dielectric constants of the metals. Extinction spectra for silver particles in aqueous solution typically give rise to a single sharp peak in the visible region, whereas the gold particle gives rise to a broad peak of lower intensity shifted to the infrared region of the spectrum [68]. Even though gold particles are less sensitive, they are frequently used for biosensing applications due to the fact that they are less likely to oxidize [69].

Size also plays an important role in the position and shape of the LSPR spectrum. When the diameter of a gold sphere increases from 9 to 99 nm, the λ_{max} shifts from approximately 520 to 580 nm [70]. The spectrum also broadens as the diameter increases because the amount of scattering increases in larger particles, leading to an overall increase in the area under the extinction peak [71]. In addition, larger particles exhibit radiation damping on faster timescales, which in turn produces broader spectral features [29,72]. Larger spheres have greater m-values, but much broader spectra, decreasing the resolution [73].

Another way to tune the LSPR spectrum is to vary the nanoparticle shape. When comparing single Ag triangular nanoprisms and spheres it was found that the spectra of the nanotriangles were more sensitive to changes in external RI than those of the spheres, consistent with ensemble measurements [74]. In a bulk RI study of nanotriangles, Sherry *et al*. found the m-values of three particles varied from 183 to 205 nm/RIU [62]. Using theoretical modeling, they found that the line widths of prism spectra increase not with volume as spheres do, but with sharpness of the corners. The sharp corners of the triangles provided enhanced electromagnetic fields on the surface and give rise to the increased sensitivity over spheres, which have an m-value of 161 nm/RIU [32]. The m-value of cubes is also greater than that of spheres, and has been measured to be 175 nm/ RIU [75].

Sensors made from gold rather than silver are more common since gold is less likely to oxidize, its biological toxicity is lower than that of silver [76,77], and the characteristic infrared λ_{max} of gold nanoparticles is less invasive for biological applications. Tuning λ_{max} through NP size and shape can be exploited to create multiplexed sensors, since nanoparticles with distinct spectra can be fabricated and each type functionalized with a different analyte probe. Recent studies have demonstrated synthesis of nanoparticles in a variety of shapes, including nanostars [78], nanooctahedrons [79] and nanodecahedrons [80]. Based on the observation that the sharp corners on triangles give the greatest field enhancement, these shapes are expected to yield unprecedented sensitivity, a truly exciting possibility for biosensing applications. Given the tunability of both the m-value and the λ_{max}, from the ultraviolet to infrared region of the spectrum, it is not surprising that LSPR has found a prominent place in biosensing.

Detecting small analytes via protein conformational changes

Since there are a growing number of diseases linked to protein misfolding, the measurement of protein conformational changes is crucial in understanding how proteins work. These measurements are commonly carried out using solution-based techniques, such as fluorescence or circular dichroism, but they require large amounts of sample, do not permit convenient sample regeneration and data analysis can be complex. Some conformational changes have been observed with SPR [21,81–83]; however, the long field-decay length makes changes in protein conformation show only minor changes in the signal. The LSPR decay length is on the same size scale as proteins; hence, when proteins change conformation they cause larger changes in the observed signal.

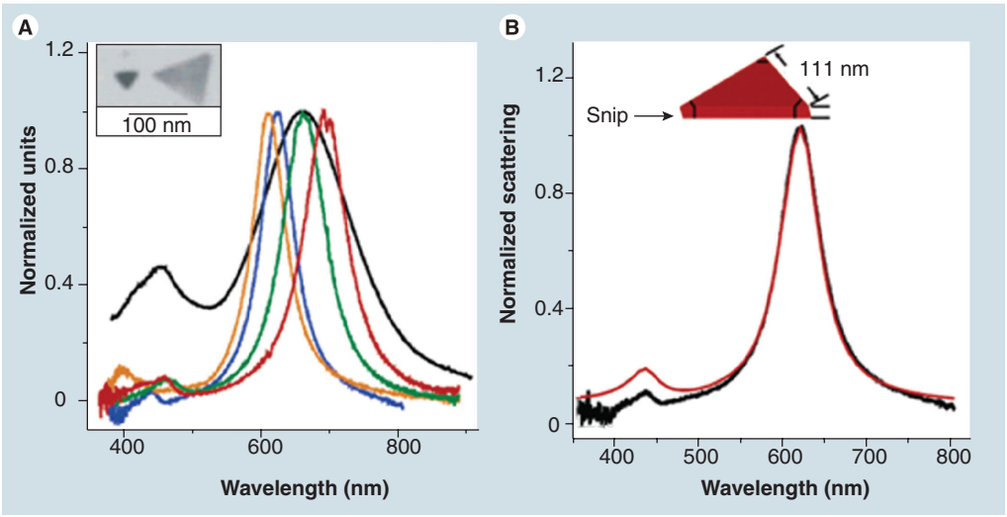

Figure 2. Localized surface plasmon resonance spectra of silver triangular nanoprisms. **(A)** Ensemble extinction spectrum (black) and single nanoparticle dark-field scattering spectra (colored) of triangular nanoprisms. A transmission electron microscopy image of representative nanoprisms is shown in the inset. **(B)** Theoretically modeled spectrum (red) and experimentally acquired spectrum (black) of a single triangular nanoprism using the DDA method. The theoretical spectrum was calculated for a nanoprism with edge length = 111 nm, snip = 15 nm and thickness = 10 nm.
Reproduced with permission from [59].

The Van Duyne group was the first to demonstrate quantitative LSPR measurements of a conformational change of calmodulin (CaM), which switches from a 'closed' to an 'open' state upon binding Ca^{2+} [84]. It is important to note that since Ca^{2+} is such a small ligand that upon binding it does not change the local RI significantly enough to give rise to an LSPR signal [7]. In this study, the CaM is covalently linked to a cutinase (Cut) domain at both the C and N termini (creating CutCaMCut), which serves to immobilize all proteins in a uniform

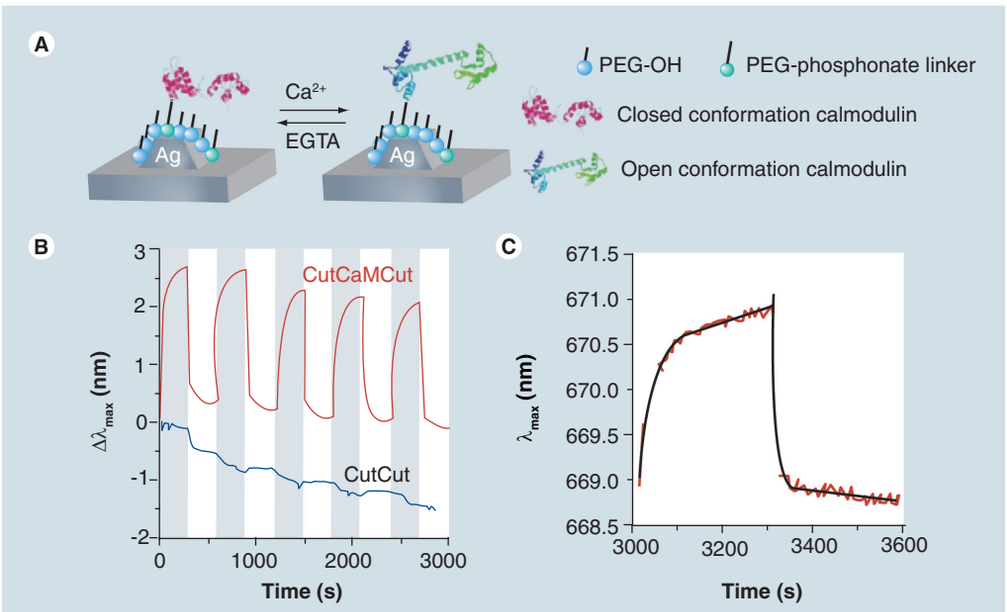

Figure 3. Calcium-modulated plasmonic sending. (A) Reversible binding of Ca^{2+} to CutCaMCut. **(B)** The shifts in the localized surface plasmon resonance spectrum ($\Delta\lambda$) over time as cycles of $CaCl_2$, grey, and EGTA (white) solutions were introduced to CutCaMCut (red) and CutCut (blue). **(C)** Sample of a $CaCl_2$/EGTA cycle showing the exponential fit of Equation 3 (black) to the experimental result (red). Cut: Cutinase.
Reproduced with permission from [7].

orientation with respect to the surface and to provide conformational flexibility. When the immobilized CutCaMCut is exposed to solution phase Ca^{2+} the conformational changes, as depicted in Figure 3A, result in a λ_{max} red shift. When a metal chelator is introduced to extract Ca^{2+} from CutCaMCut, λ_{max} blue shifts back to approximately the original value, as shown in Figure 3B. Control experiments confirm these shifts only occur when CaM is present. The red shifts in the presence of Ca^{2+} indicate an increase in the RI near the silver surface, meaning CutCaMCut reorients on the surface at a higher packing density within the sensing volume. The time resolved data, shown in Figure 3C, was fit to Equation 4 where t is time in seconds, $\lambda_{max\,(0)}$ is the initial λ_{max} value, τ is the rate of change in seconds, and A and B are scaling factors. From this fit the rate constants of approximately 0.034 and 0.127 s^{-1} were determined for the opening and closing processes, respectively.

$$\lambda_{max} = \lambda_{max(0)} + Ae^{-t/\tau} + B * t \quad (4)$$

This study highlights how the localized sensing volume of LSPR can be exploited to measure protein conformational changes in real time. LSPR is label-free, requires small sample volumes, makes it possible to easily regenerate the sample, and enables the detection of small molecules that are difficult to detect using other label-free techniques. In the current design, this method could only detect Ca^{2+} ions in the micromolar range, which is not as good as electrochemical methods [85]. However, the range is useful in biological systems where cellular calcium concentrations are typically in the micromolar range. LSPR can detect small molecules in other ways as well; one other example, which exploits the resonant effect, is discussed in the following section.

Resonance-enhanced LSPR

A challenge for plasmonic sensing is detecting small molecules since they do not significantly alter the local RI upon binding. Recently, SPR measurements of drug binding to surface-tethered human serum albumin yielded a signal that was 1000-times smaller than the signal for human serum albumin binding to surface-tethered drugs [86]. However, when the analyte is a chromaphore, displaying a strong extinction coefficient near the LSPR of the sensor surface, it is quite easy to detect. The chromophore increases the λ_{max} shift via the resonant effect, which was first investigated by Pockrand *et al*. in 1978 for SPR and by Haes *et al.* for LSPR in 2006 [87,88]. This enhancement is strongly affected by the real part of the wavelength-dependent RI of the analyte, which resonates with the localized surface plasmons; the resulting shifts can be predicted theoretically using this model [28,87,88]. A study of rhodamine 6G (R6G) adsorbed on silver nanoprisms revealed that the enhancement of LSPR peak shifts as a function of wavelength contained three peaks, even though the wavelength-dependent UV-Vis spectra of R6G contains only two peaks [89]. These features result from different adsorbed forms of R6G on the surface. Hence, chromophore analytes do not just enhance the LSPR shift, but can also provide information regarding the way that analytes adsorb on nanoparticle surfaces.

Zhao *et al.* were the first to exploit the resonant effect for biosensing [90]. They examined the interaction of an inhibitor and a substrate, both small molecules, with immobilized bacterial CYP101, a member of the cytochrome p450 family that helps metabolize drugs in the liver [91]. The CYP101 protein contains a heme chromophore that has a strong absorption at approximately 417 nm, which red shifts by 8 nm when an inhibitor is bound and blue shifts by 27 nm when a substrate is bound [92–94]. A schematic of this binding is depicted in Figure 4 along with a plot of LSPR peak shift as a function of the sensor's LSPR λ_{max} for both the inhibitor, imidazole, and the substrate, camphor, and representative LSPR spectra before and after each type of binding. When imidazole binds, the local RI increases, causing a red shift in λ_{max}, which is enhanced by the red shift of the heme absorption. When camphor is bound, the local RI also increases causing a red shift in λ_{max}; however, this is overwhelmed by the blue shift of the heme absorption spectrum leading to a blue shift of λ_{max}. When λ_{max} of the nanoparticle substrate was tuned so the LSPs resonated the peak of the heme, the magnitude of the shift increased for binding of both camphor and imidazole.

The resonant effect has even been used to enhance LSPR studies of drugs binding to human CYP3A4 cytochrome p450 protein [95]. The drugs that bind CYP3A4 are classified into types: type I causes a blue shift in a certain heme absorption peak and type II cause a red shift in this peak [93]. The resonant effect was able to distinguish between type I and II drug binding, as shown in Figure 5, despite the fact that the LSPR peak is far from the heme's absorption peak.

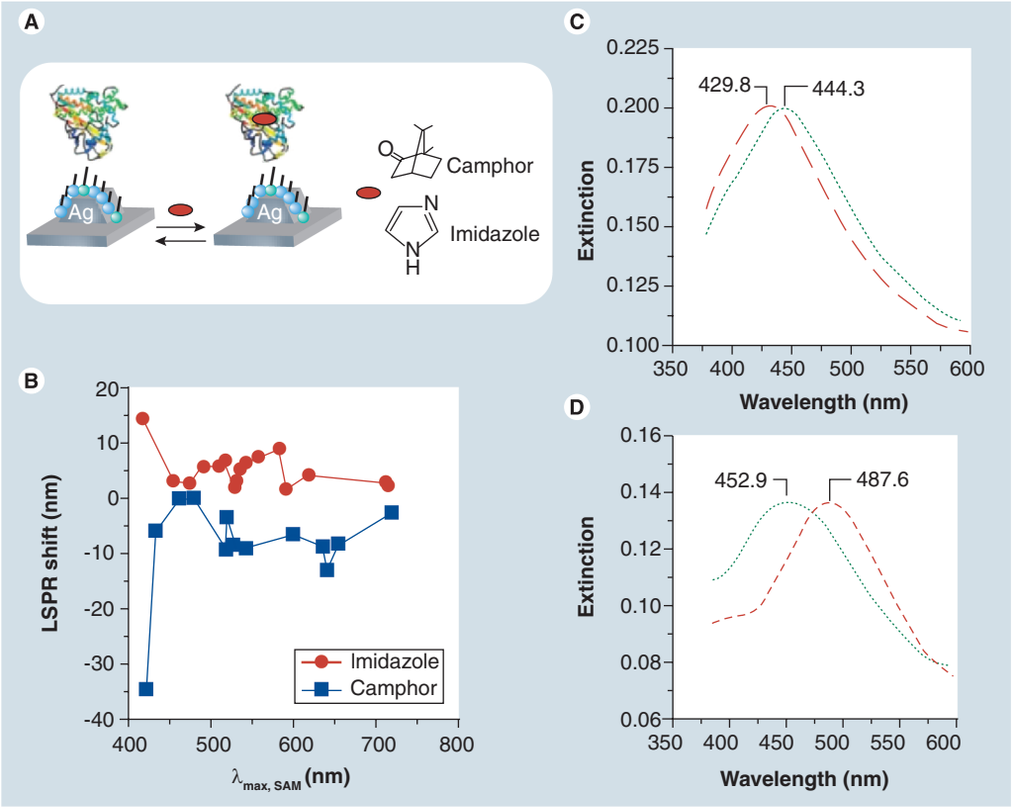

Figure 4. Substrate binding to cytochrome P450. (A) Camphor or imidazole binding to CYP101 protein tethered to mercaptoundecanoic acid on a Ag nanosphere lithography substrate. **(B)** Localized surface plasmon resonance shifts from imidazole (red) and camphor (blue) as a function of Ag nanosphere lithography substrate λ*max*. **(C)** Extinction spectrum of CYP101 on Ag nanosphere lithography substrate before (pink dashed) and after (green dotted) imidazole incubation. **(D)** Extinction spectrum of CYP101 on Ag nanosphere lithography substrate before (pink dashed) and after (green dotted) camphor incubation.
LSPR: Localized surface plasmon resonance.
Reproduced with permission from [80].

This study demonstrates that the resonance effect not only improves the magnitude of the signal, but can also be used to identify the type of bound ligand in certain cases.

By tuning the λ_{max} position of the LSPR sensor to match with the absorption peak of chromophoric analytes, the LSPR peak can be maximally enhanced. The examples presented in this section demonstrate that it can: increase the magnitude in λ_{max} shift, enabling sensing of small molecules, which are normally undetectable; provide information about the adsorption state of an analyte of interest; and identify the type of analyte bound in specific instances. This increased sensitivity makes resonant LSPR one of the most sensitive techniques for detecting small analyte binding. Although resonant LSPR can identify the type of drug bound to a probe, further identification of the bound analyte can be provided by combining LSPR with other techniques, such as mass spectrometry (MS) described in the next section.

Combined MS & LSPR

Localized surface plasmon resonance biosensors can measure a wide variety of biomolecular interactions because almost every interaction causes a change in the local RI. This can be a drawback, as the sensor cannot distinguish between capturing the analyte of interest and general fouling of the surface. Moreover, analytes of different makeup but similar functionality cannot be distinguished by LSPR measurements alone. Combining LSPR with MS is one solution to this problem. In this combined technique, the amount of analyte bound is quantitated by LSPR and the analyte is identified by MS. This is valuable in cases where there is nonspecific binding to the probes or surface and where multiple analytes are being monitored simultaneously. While combining MS with sensing is not novel, the increased specificity offered by this system greatly enhances the potential of LSPR to function as a multiplexed sensor for any panel of analytes.

The Van Duyne group developed an LSPR biosensor capable of detecting amyloid derived diffusible ligands (ADDLs), a biomarker for Alzheimer's disease, down to picomolar concentrations [59,96]. Anker *et al.* pioneered combining matrix-assisted laser desorption/ionization MS with LSPR in order to identify ADDLs, as illustrated in Figure 6 [97]. The ADDL binding was observed in real-time, see Figure 6B, and the MS spectrum (Figure 6C) confirmed the presence of the ADDL building block, Aβ. The MS results showed Aβ was present in both an oxidized and a reduced form, which was hypothesized to be important for Alzheimer's disease progression. The resolution of the two different Aβ forms could not have been determined using LSPR as both forms shift λ_{max} by the same amount. By identifying the subtle, but important, difference in Aβ monomers that make up ADDLs, Anker *et al.* have demonstrated the power of the combined LSPR/MS technique. This technique would be ideal to evaluate the specificity of different probes on a multiplexed sensor. LSPR multiplexed sensors are capable of reaching new levels of miniaturization using SNP LSPR sensing, which is discussed in detail in the following sections.

SNP LSPR

The studies in the 'Multiplexed biological imaging using LSPR' section focused primarily on the link between physical and spectral properties of SNPs [28,29]. While understanding these correlations is important, another advantage of SNP spectroscopy is its improved LSPR sensing capabilities. SNP measurements possess all the advantages of ensemble LSPR measurements, as well as several other noteworthy advantages for biosensing:

- SNP spectroscopy has the ability to greatly increase the sensitivity of biological sensing applications, as described in the next paragraph [28,74,98];
- Since only a few nanoparticles need to be monitored at a time, the required sample volume (in the attoliter range) is significantly lower than it is for ensemble methods;

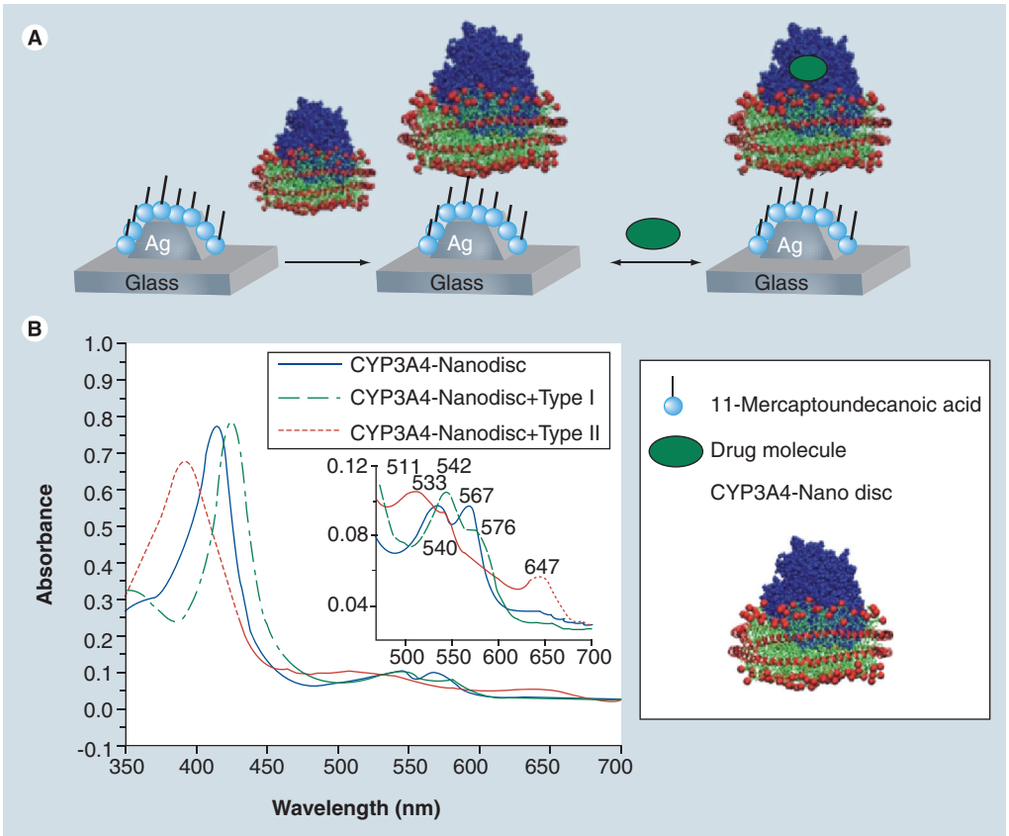

Figure 5. Drug screening with human cytochrome P450. (A) CYP343 in a Nanodisc binding to mercaptoundecanoic acid functionalized Ag nanoparticle followed by drug binding to CYP343. **(B)** Absorbance spectra of CYP343/Nanodisc sensor without any drug (blue solid) with type I drug bound (red dotted) and with type II drug bound (green dashed).
Reproduced with permission from [85].

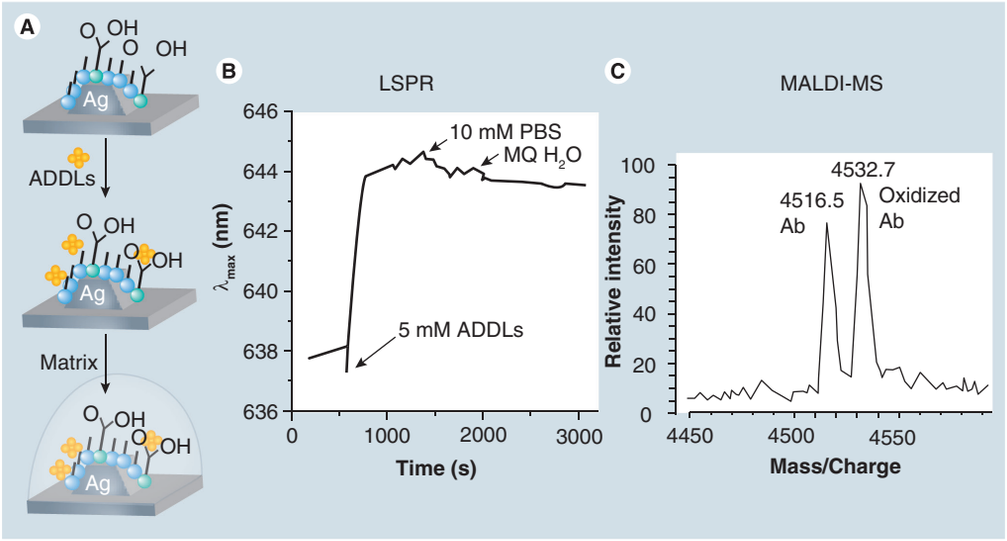

Figure 6. Combining LSPR and MALDI MS. (A) ADDLs binding to nanosphere lithography substrate followed by coating with sinapinic acid. **(B)** Real-time plot of ADDLs binding. **(C)** MALDI-TOF-MS spectrum of ADDLs.
ADDL: Amyloid-derived diffusible ligand; LSPR: Localized surface plasmon resonance; PBS: Phosphate buffered saline.
Reproduced with permission from [87].

- Multiple nanoparticles, each with a unique λ_{max}, can be monitored simultaneously with this platform, making it readily amenable to multiplexing [71,99,100];
- The motion of each nanoparticle can be tracked in real-time allowing the trajectory to be determined in biologically amenable solutions;
- Plasmonic nanoparticles offer advantages for biological imaging since they are not susceptible to photobleaching. In the remainder of this article we describe studies that have demonstrated these superior sensing capabilities of SNP LSPR methods.

As discussed in the 'LSPR fundamentals' section, the LSPR signal is due to an analyte displacing solvent near the sensor surface, hence changing the effective RI around the nanoparticles. In ensemble LSPR one must change the RI around all particles in an array to observe a shift in λ_{max}. However, in single particle LSPR the RI only needs to be changed around one nanoparticle, significantly reducing the number of analyte molecules required to produce an observable signal. McFarland *et al.* were the first to observe formation of a self-assembled monolayer on a single silver sphere in real-time with LSPR [30]. A self-assembled monolayer of 1-hexadecanethiol produced a 40.7 nm λ_{max} shift (Figure 7). Based on the known thiol self-assembled monolayer packing density on silver and the approximate nanoparticle surface area, calculations estimate that this signal results from only 6×10^4 molecules adsorbed on the nanoparticle, or approximately 100 zeptomole sensitivity. Since then, other studies have focused on biosensing with SNP LSPR. Haes *et al.* observed a shift of 12.7 nm when streptavidin bound to a biotinylated silver sphere; this response is estimated to result from binding of fewer than 700 molecules of streptavidin [35]. Similarly, Raschke *et al.* measured streptavidin

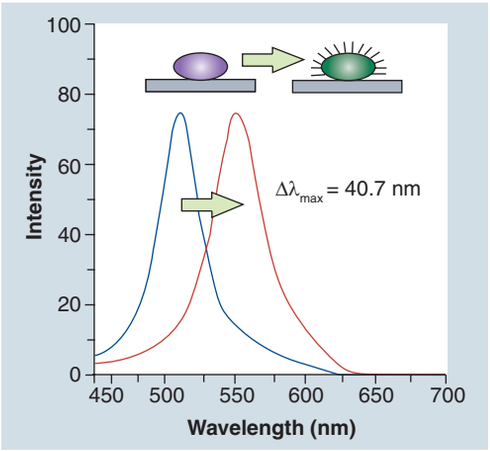

Figure 7. Single nanoparticle localized surface plasmon resonance sensing.
Localized surface plasmon resonance scattering spectra of a single Ag nanoparticle before (blue) and after (red) immobilization of 1-hexadecanethiol self-assembled monolayer. Spectra were collected in N_2.
Reproduced with permission from [28].

binding to biotinylated-bovine serum albumin coated gold nanoparticles with a different passivating layer and were able to observe a signal of only 1.19 nm corresponding to fewer than 70 molecules binding to the surface [101]. In this work, they monitored the λ_{max} shift as a function of time, and could fit the data to a first order kinetic model. More recently, Chen *et al.* developed a robust LSPR-based assay for measuring enzymatic catalysis with SNPs [102]. This assay was able to detect only a few horseradish peroxidase molecules per nanoparticle. These significantly improved detection limits demonstrate possibly the greatest advantage of SNP over ensemble LSPR.

As these studies show, SNP LSPR is able to detect a very small number of molecules and due to the small size of nanoparticles, this requires very small quantities of sample. Hence, LSPR is convenient for medical testing and diagnostics as it minimizes the amount of blood, or other biological fluid, that must be collected from a patient. Another advantage of miniaturization is that SNP LSPR lends itself to multiplexed sensing. The next section focuses on describing one type of LSPR multiplexing that measures both the plasmon resonance wavelength and the nanoparticle position in 2D, simultaneously.

Multiplexed SNP tracking

Single particle tracking, where the trajectory of an individual particle can be mapped, has long been established as a means to study motion in biological systems. Tracking has employed many types of particles, including fluorescent particles, latex beads and gold colloids [103]. These studies have succeeded at monitoring receptor diffusion on membranes and in cells, identifying corrals formed by cytoskeletal proteins near membranes and measuring biological motion [104–106]. Employing nanoparticles for biological imaging allows long time observation as they do not photobleach or blink [107]. If plasmonic nanoparticles are used, the λ_{max} shift can be exploited to provide more information. For example, plasmonic nanoparticles have been used to monitor agglomeration of labeled receptors as a function of time since the coupling of surface plasmons cause large λ_{max} shifts [105].

Recently, Bingham *et al.* combined single particle tracking and LSPR spectroscopy to allow the simultaneous acquisition of the particle trajectory and shifts in the particle λ_{max}, which yields information on the corresponding local environments [108]. The instrument they developed employs the dark-field microscopy apparatus shown in Figure 8. Wide-field images of many particles were obtained as a function of λ_{max} and time. The scattering spectra of three different nanoparticles are presented in Figure 9A and their trajectory in a highly viscous solution with is shown in Figure 9B. The fits in Figure 9C are consistent with Brownian motion in 2D. Diffusion constants were determined by fitting, and were used to calculate the estimated size of each nanoparticle; the nanoparticle sizes calculated agree well with those measured with transmission electron microscopy [109].

This work not only illustrates improved particle tracking capabilities, but, more importantly, it paves the way for advanced biophysical work involving the analysis of multiple interacting nanoparticles simultaneously. For example, if both the antibody and antigen of a binding pair are tethered to a nanoparticle, there should be a significant change in diffusion rate and the λ_{max} when they bind, which should permit sensing on the single molecule scale. In addition, measurements of this type should also give rise to highly sensitive, miniaturized multiplexing. As mentioned above, it is possible to modulate the λ_{max} position for a nanoparticle by varying the size and shape of the particle. It has been shown by Xu *et al.* and Bingham *et al.* that multiple particles can be spectrally resolved simultaneously in an imaging format [107,108]. The exciting expansion of this work into a multiplexed imaging scheme is discussed in the next section.

Multiplexed biological imaging using LSPR

Since each individual nanoparticle can possess unique LSPR spectral properties as well as specific biological functionalization, ensemble measurements of these particles could be quite useful in multiplexed imaging, diagnostics and therapeutics. Furthermore, both the plasmonic particles themselves and the detection instrumentation are noninvasive, allowing for multiplexed *in vivo* studies. This type of multiplexed imaging offers a major advantage for biological systems, as many disease-related phenomena involve more than one component. Moreover, a library of nanoparticles with different λ_{max} could each contain a different drug of choice, introducing the possibility of carrying out therapeutic applications in which specific cells can be targeted by multiple drugs for maximum efficacy.

One of the first studies demonstrating the concept of using nanoparticles of different plasmonic properties for multiplexed detection was carried out by Taton *et al* [110]. In this study, multiple spectrally distinct nanoparticles were functionalized with different oligonucleotides to afford multiplexed detection of DNA microarrays. The idea of plasmonic multiplexing has been extended in recent studies to include *in vivo* imaging of biological tissue and cells for medical diagnostics [111–113]. The lack of photobleaching, low background in biological samples, and a large scattering cross-section of nanoparticles make LSPR imaging ideal for *in vivo* sensing and facilitates combined imaging and targeted therapeutic delivery. Recent studies have demonstrated the use of plasmonic nanoparticles to simultaneously image and kill diseased cells in a targeted manner using light-generated heat and reactive oxygen species [114,115]. Other studies have coated the surface of the nanoparticle with drug-carrying agents, such as polymers or peptides, which provide controlled release over time [116–118]. An additional therapeutic avenue used plasmonic nanoparticles containing DNA to influence gene expression *in vivo* [119].

These studies demonstrate that multiplexed LSPR imaging can be applied in new and inventive ways to improve diagnostics and therapeutics. The use of spectrally distinct nanoparticles allows a wide array of molecules of interest to be tethered to different nanoparticles, providing multiplexed biological recognition. In addition, with plasmonic nanoparticles there are several ways for therapeutic molecules to be transported to, and released at, a specific location. The ability to track and manipulate plasmonic nanoparticles in real time should greatly aid *in vivo* diagnostics and therapeutics. In this application, changes in the LSPR spectra can be exploited to confirm biological recognition and that drug release has occurred.

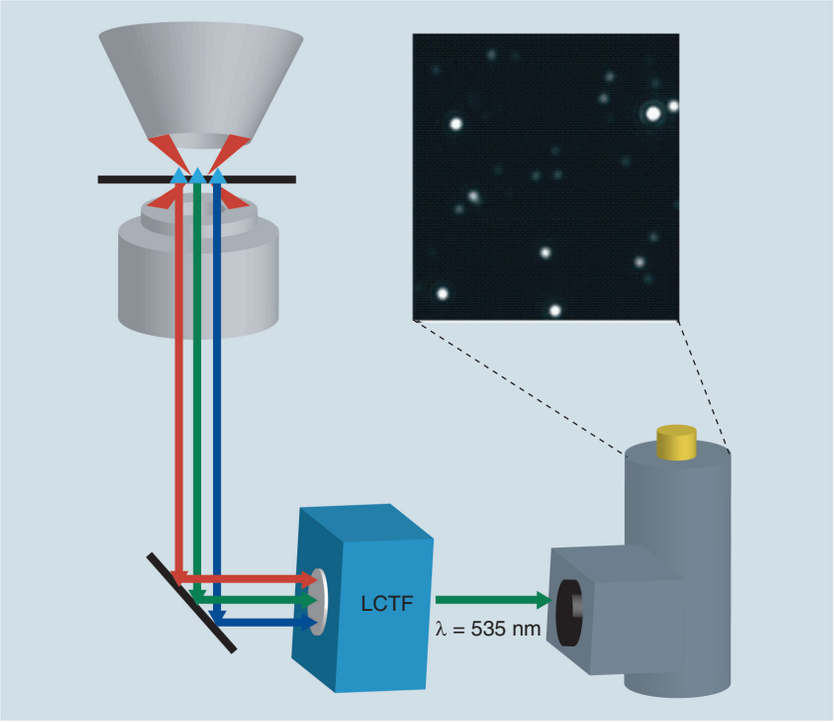

Figure 8. Wide-field single nanoparticle localized surface plasmon resonance apparatus. An inverted microscope with a dark field condenser shines light on silver nanoparticles and only the scattered light is collected by an oil-immersion objective. The LCTF selects one wavelength to transmit at a time.
LCTF: Liquid crystal tunable filter.
Reproduced with permission from [97].

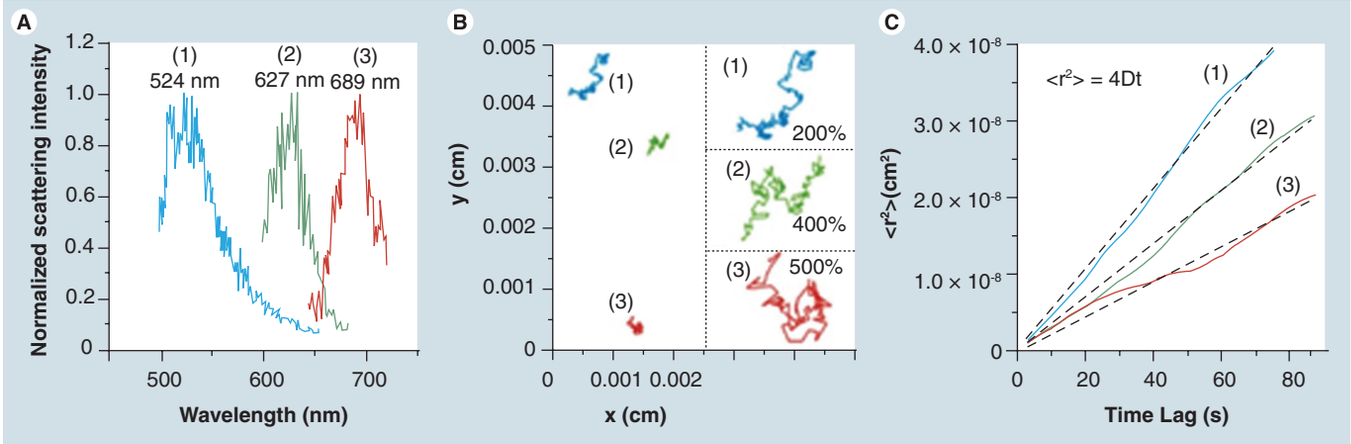

Figure 9. Characterization moving nanoparticles. (A) Scattering spectra of three different silver nanoparticles taken using the wide-field localized surface plasmon resonance imaging apparatus. **(B)** Diffusion trajectories of the nanoparticles. Insets are magnified depictions of each trajectory. **(C)** Plot of mean square displacement vs time lag. The approximate size of the nanoparticle is determined from linear fits to this data.
Reproduced with permission from [97].

Conclusion

This article has highlighted recent advances in LSPR spectroscopic biosensing. LSPR measurements require simple, inexpensive instrumentation and can use a variety of flexible signal transduction platforms. By varying the material, size and shape of the nanoparticles that comprise the sensor, both the λ_{max} position and the RI sensitivity can be tuned. Both protein conformational changes as well as the resonant effect have enabled sensing of small molecules that would ordinarily be below the detection limits of LSPR. Furthermore, unambiguous identification of biological analytes on the sensor surface can be achieved by combining LSPR with MS. By monitoring SNPs, detection limits can be improved, nanoscale multiplexed sensors can be made and particles can be tracked in real-time. Thus, LSPR-based biosensing is a powerful platform for the most challenging problems in biomedicine.

Future perspective

Localized surface plasmon resonance-based biosensing devices offer many advantages over more traditional biological assays: instrumentation and device design is inexpensive; a variety of signal transduction platforms are available, which can be surface bound, or free to diffuse in solution; all platforms are easily functionalized with any probe of interest; the probes can be conveniently regenerated by sensor rinsing; and the nano-size of the sensor means small quantities of sample are required for sensing. Furthermore, microfluidics can be incorporated into LSPR imaging formats to create convenient, multiplexed delivery of many samples, or tethering of many probes, to the sensor. Such multiplexed arrays are ideal for creating diagnostics based on multiple biomarkers and for screening potential therapeutic molecules in drug development. Multiplexed sensing can even be carried out for unknown analytes as the combination of

Executive summary

Localized surface plasmon resonance fundamentals

- Localized surface plasmon resonance (LSPR) spectroscopy is widely applicable for biosensing due to the simple, low-cost instrumentation and the variety of signal transduction platforms that can be used.
- LSPR biosensing makes use of the fact that plasmonic nanoparticles are sensitive to local changes in refractive index and hence no labeling of analytes is needed.

Correlated physical & optical properties of nanoparticles

- The LSPR wavelength position and sensitivity to the environment refractive index can be tuned by varying the nanoparticle material, size, and shape.
- Single nanoparticle LSPR has recently been used to define more detailed correlations between the physical and optical properties of plasmonic nanoparticles.

Detecting small analytes via protein conformational changes

- It has been demonstrated that LSPR can detect protein conformational changes in real-time.
- Small molecules that induce protein conformational changes can be detected as a result, even though they are typically below the LSPR detection limit.

Chromophore enhanced LSPR

- Small molecules can be detected by taking advantage of the resonant effect.
- Different analytes can be distinguished based on the direction of the LSPR shift upon binding to a chromophoric probe protein.

Combined mass spectrometry & LSPR

- Mass spectrometry has been combined with LSPR to unambiguously identify surface-bound analytes, something that cannot be done by plasmonic sensing alone.

Single nanoparticle LSPR

- LSPR biosensing with single nanoparticles has the ability to greatly increase the sensitivity and allow for advanced multiplexing applications.
- Single nanoparticle sensing has lowered detection limits to zeptomole levels for alkanethiols and even lower, approximately 70 molecules, for the protein streptavidin.

Multiplexed individual nanoparticle tracking

- Multiplexed, single molecule sensing has demonstrated the ability to simultaneously monitor the position and LSPR spectrum of many nanoparticles.
- This not only lays the groundwork for significantly better miniaturization of multiplexed sensors, but also allows motion to be correlated with the refractive index of a local environment.

Multiplexed biological imaging using LSPR

- Biological imaging can be improved by taking advantage of the large scattering coefficients and nonbleaching characteristics of plasmonic particles.
- Biological imaging and drug delivery can be carried out in a multiplexed format, making use of different colored plasmonic particles.

MS or surface-enhanced Raman spectroscopy (not discussed here) with LSPR provides unambiguous analyte identification after the binding event has occurred.

Single particle LSPR offers many exciting prospects for miniaturized biosensing devices. Combining single particle wide-field imaging with microfluidics will allow for an unprecedented number of processes to be measured simultaneously on-chip. Multiplexed biophysical studies involving LSPR imaging and tracking can greatly aid our understanding of disease-related phenomena, particularly those involving more than one component. This type of imaging device can also be expanded to include surface-enhanced Raman imaging by labeling biomarkers of interest with commercially available (Oxonica Inc.) Raman-active tags. Each tag is identified by the unique, sharp Raman spectrum of an incorporated molecule, making these tags ideal for multiplexed applications [120]. Finally, because plasmonic particles are easily functionalized to reduce an immune response, it is expected that multiplexed biosensing *in vivo* will show increased popularity in the future [121].

Financial & competing interests disclosure

The authors gratefully acknowledge support from the National Science Foundation (Grants EEC-0647560, CHE-0911145, DMR-0520513, and BES-0507036), the NIH (4 R56 Grant 5R56DK078691–02), the Defense Advanced Research Projects Agency (Grant FA9550–08–1–0221/P00003) and the National Cancer Institute (1 U54 CA119341–01). The authors have no other relevant affiliations or financial involvement with any organization or entity with a financial interest in or financial conflict with the subject matter or materials discussed in the manuscript apart from those disclosed.

No writing assistance was utilized in the production of this manuscript.

Bibliography

Papers of special note have been highlighted as:
- ▪ of interest
- ▪▪ of considerable interest

1 Hess ST, Huang SH, Heikal AA, Webb WW. Biological and chemical applications of fluorescence correlation spectroscopy: a review. *Biochemistry (Mosc.)* 41(3), 697–705 (2002).

2 Zsila F, Bikadi Z, Simonyi M. Induced circular dichroism spectra reveal binding of the antiinflammatory curcumin to human α(1)-acid glycoprotein. *Biorg. Med. Chem.* 12(12), 3239–3245 (2004).

3 Patra D. Synchronous fluorescence based biosensor for albumin determination by cooperative binding of fluorescence probe in a supra-biomolecular host-protein assembly. *Biosens. Bioelectron.* 25(5), 1149–1154 (2010).

4 Maiti TK, Ghosh KS, Debnath J, Dasgupta S. Binding of all-trans retinoic acid to human serum albumin: fluorescence, FT-IR and circular dichroism studies. *Int. J. Biol. Macromol.* 38(3–5), 197–202 (2006).

5 Sprague BL, Pego RL, Stavreva DA, McNally JG. Analysis of binding reactions by fluorescence recovery after photobleaching. *Biophys. J.* 86(6), 3473–3495 (2004).

6 Van Duyne RP, Haes AJ, McFarland AD. Nanoparticle optics: sensing with nanoparticle arrays and single nanoparticles. *Proc. SPIE – Int. Soc. Opt. Engin.* 5223, 197–207 (2003).

7 Hall WP, Anker JN, Lin Y *et al.* A calcium-modulated plasmonic switch. *J. Am. Chem. Soc.* 130(18), 5836–5837 (2008).

▪▪ **For the first time, small molecule detection using protein conformational changes was performed using high-resolution localized surface plasmon resonance (LSPR).**

8 Hodneland CD, Lee YS, Min DH, Mrksich M. Selective immobilization of proteins to self-assembled monolayers presenting active site-directed capture ligands. *Proc. Natl Acad. Sci. USA* 99(8), 5048–5052 (2002).

9 Gurard-Levin ZA, Mrksich M. The activity of HDAC8 depends on local and distal sequences of its peptide substrates. *Biochemistry (Mosc.)* 47(23), 6242–6250 (2008).

10 Grote J, Dankbar N, Gedig E, Koenig S. Surface plasmon resonance/mass spectrometry interface. *Anal. Chem.* 77(4), 1157–1162 (2005).

11 Shin YB, Lee JM, Park MR *et al.* Analysis of recombinant protein expression using localized surface plasmon resonance (LSPR). *Biosens. Bioelectron.* 22(9–10), 2301–2307 (2007).

12 Endo T, Kerman K, Nagatani N *et al.* Multiple label-free detection of antigen-antibody reaction using localized surface plasmon resonance-based core-shell structured nanoparticle layer nanochip. *Anal. Chem.* 78(18), 6465–6475 (2006).

13 Kleinman HK, Cannon FB, Laurie GW *et al.* Biological-activities of laminin. *J. Cell. Biochem.* 27(4), 317–325 (1985).

14 Naldini L, Vigna E, Bardelli A *et al.* Biological activation of Pro-Hgf (Hepatocyte growth-factor) by Urokinase is controlled by a stoichiometric reaction. *J. Biol. Chem.* 270(2), 603–611 (1995).

15 Bagramyan K, Barash JR, Arnon SS, Kalkum M. Attomolar detection of botulinum toxin type A in complex biological matrices. *PLoS ONE* 3(4), e2041 (2008).

16 Lee HJ, Wark A, Corn RM. Enzymatic manipulation of surface biomolecular nanostructures for the detection of bioaffinity interactions with SPR imaging and fluorescence measurements. *Abs. Papers Am. Chem. Soc.* 231 (2006).

17 Homola J, Yee SS, Gauglitz G. Surface plasmon resonance sensors: review. *Sensors Actuators B: Chem.* 54(1–2), 3–15 (1999).

18 McDonnell JM. Surface plasmon resonance: towards an understanding of the mechanisms of biological molecular recognition. *Curr. Opin. Chem. Biol.* 5(5), 572–577 (2001).

19 Lee HJ, Wark AW, Corn RM. Enhanced bioaffinity sensing using surface plasmons, surface enzyme reactions, nanoparticles and diffraction gratings. *Analyst* 133(5), 596–601 (2008).

20 Willets KA, Van Duyne RP. Localized surface plasmon resonance spectroscopy and sensing. *Ann. Rev. Phys. Chem.* 58, 267–297 (2007).

▪ **This review is an excellent detailed description on the mathematical foundations of LSPR and its early biosensing experiments.**

21 Sota H, Hasegawa Y, Iwakura M. Detection of conformational changes in an immobilized protein using surface plasmon resonance. *Anal. Chem.* 70(10), 2019–2024 (1998).

22 Brighamburke M, Edwards JR, Oshannessy DJ. Detection of receptor ligand interactions using surface-plasmon resonance – model studies employing the Hiv-1 Gp120/Cd4 Interaction. *Anal. Biochem.* 205(1), 125–131 (1992).

23 Rickert J, Brecht A, Gopel W. Quartz crystal microbalances for quantitative biosensing and characterizing protein multilayers. *Biosens. Bioelectron.* 12(7), 567–575 (1997).

24 Cao Z, Jiang X, Meng W *et al.* An EQCM study on the interaction of heparin with the charge-transfer complex generated during o-tolidine electrooxidation: a biosensing mode with a dynamically renewed surface. *Biosens. Bioelectron.* 23(3), 348–354 (2007).

25 Zheng GF, Patolsky F, Cui Y, Wang WU, Lieber CM. Multiplexed electrical detection of cancer markers with nanowire sensor arrays. *Nat. Biotechnol.* 23(10), 1294–1301 (2005).

26 Zheng GF, Gao XPA, Lieber CM. Frequency domain detection of biomolecules using silicon nanowire biosensors. *Nano Lett.* 10(8), 3179–3183 (2010).

27 Keren K, Berman RS, Buchstab E, Sivan U, Braun E. DNA-templated carbon nanotube field-effect transistor. *Science* 302(5649), 1380–1382 (2003).

28 Klar T, Perner M, Grosse S *et al.* Surface-plasmon resonances in single metallic nanoparticles. *Phys. Rev. Lett.* 80(19), 4249–4252 (1998).

29 Sönnichsen C, Franzl T, Wilk T *et al.* Drastic reduction of plasmon damping in gold nanorods. *Phys. Rev. Lett.* 88(7), 077402 (2002).

30 McFarland AD, Van Duyne RP. Single silver nanoparticles as real-time optical sensors with zeptomole sensitivity. *Nano Lett.* 3(8), 1057–1062 (2003).

31 Yguerabide J, Yguerabide EE. Light-scattering submicroscopic particles as highly fluorescent analogs and their use as tracer labels in clinical and biological applications – I. Theory. *Anal. Biochem.* 262(2), 137–156 (1998).

32 Haynes CL, Van Duyne RP. Nanosphere lithography: a versatile nanofabrication tool for studies of size-dependent nanoparticle optics. *J. Phys. Chem. B.* 105(24), 5599–5611 (2001).

33 Haes AJ, Van Duyne RP. A nanoscale optical blosensor: sensitivity and selectivity of an approach based on the localized surface plasmon resonance spectroscopy of triangular silver nanoparticles. *J. Am. Chem. Soc.* 124(35), 10596–10604 (2002).

34 Hulteen JC, Van Duyne RP. Nanosphere lithography – a materials general fabrication process for periodic particle array surfaces. *J. Vac. Sci. Technol. A.* 13(3), 1553–1558 (1995).

35 Haes AJ, Stuart DA, Nie SM, Van Duyne RP. Using solution-phase nanoparticles, surface-confined nanoparticle arrays and single nanoparticles as biological sensing platforms. *J. Fluoresc.* 14(4), 355–367 (2004).

36 Thaxton CS, Mirkin CA. Plasmon coupling measures up. *Nat. Biotechnol.* 23(6), 681–682 (2005).

37 Chah S, Hammond MR, Zare RN. Gold nanoparticles as a colorimetric sensor for protein conformational changes. *Chem. Biol.* 12(3), 323–328 (2005).

38 Reinhard BM, Siu M, Agarwal H, Alivisatos AP, Liphardt J. Calibration of dynamic molecular rule based on plasmon coupling between gold nanoparticles. *Nano Lett.* 5(11), 2246–2252 (2005).

39 Reinhard BM, Sheikholeslami S, Mastroianni A, Alivisatos AP, Liphardt J. Use of plasmon coupling to reveal the dynamics of DNA bending and cleavage by single EcoRV restriction enzymes. *Proc. Natl Acad. Sci. USA* 104(8), 2667–2672 (2007).

40 Freestone I, Meeks N, Sax M, Higgitt C. The Lycurgus Cup – a Roman nanotechnology. *Gold Bull.* 40(4), 270–277 (2007).

41 Dahlin AB, Tegenfeldt JO, Hook F. Improving the instrumental resolution of sensors based on localized surface plasmon resonance. *Anal. Chem.* 78(13), 4416–4423 (2006).

42 Yonzon CR, Stuart DA, Zhang XY *et al.* Towards advanced chemical and biological nanosensors – An overview. *Talanta* 67(3), 438–448 (2005).

43 Atwater H. The promise of plasmonics. *Sci. Am.* 296, 56–63 (2007).

44 Ozbay E. Plasmonics: merging photonics and electronics at nanoscale dimensions. *Science* 311(5758), 189–193 (2006).

45 Stiles PL, Dieringer JA, Shah NC, Van Duyne RR. Surface-enhanced Raman spectroscopy. *Ann. Rev. Anal. Chem.* 1, 601–626 (2008).

46 Stockle RM, Suh YD, Deckert V, Zenobi R. Nanoscale chemical analysis by tip-enhanced Raman spectroscopy. *Chem. Phys. Lett.* 318(1–3), 131–136 (2000).

47 Sundaramurthy A, Schuck PJ, Conley NR *et al.* Toward nanometer-scale optical photolithography: utilizing the near-field of bowtie optical nanoantennas. *Nano Lett.* 6(3), 355–360 (2006).

48 Zhang X, Liu Z. Superlenses to overcome the diffraction limit. *Nat. Mater.* 7, 435–441 (2008).

49 Bohren CF, Huffman DR (Eds). *Absorption and Scattering of Light by Small Particles*. Wiley, NY, USA (1983).

50 Eustis S, El-Sayed MA. Why gold nanoparticles are more precious than pretty gold: noble metal surface plasmon resonance and its enhancement of the radiative and nonradiative properties of nanocrystals of different shapes. *Chem. Soc. Rev.* 35(3), 209–217 (2006).

51 Kelly KL, Coronado E, Zhao LL, Schatz GC. The optical properties of metal nanoparticles: the influence of size, shape, and dielectric environment. *J. Phys. Chem. B.* 107(3), 668–677 (2003).

52 Van Duyne RP. Molecular plasmonics. *Science* 306(5698), 985–986 (2004).

53 Haes AJ, Van Duyne RP. A unified view of propagating and localized surface plasmon resonance biosensors. *Anal. Bioanal. Chem.* 379(7–8), 920–930 (2004).

54 Mie G. Articles on the optical characteristics of turbid media, especially colloidal metal solutions. *Ann. Phys. (Letpz.)* 35, 377–445 (1908).

55 Aden AL, Kerker M. Scattering of electromagnetic waves from 2 concentric spheres. *J. Appl. Phys.* 22(10), 1242–1246 (1951).

56 Link S, El-Sayed MA. Spectral properties and relaxation dynamics of surface plasmon electronic oscillations in gold and silver nanodots and nanorods. *J. Phys. Chem. B.* 103(40), 8410–8426 (1999).

57 Jensen TR, Duval ML, Kelly KL *et al.* Nanosphere lithography: effect of the external dielectric medium on the surface plasmon resonance spectrum of a periodic array of sliver nanoparticles. *J. Phys. Chem. B.* 103(45), 9846–9853 (1999).

58 Miller MM, Lazarides AA. Sensitivity of metal nanoparticle surface plasmon resonance to the dielectric environment. *J. Phys. Chem. B.* 109(46), 21556–21565 (2005).

59 Haes AJ, Chang L, Klein WL, Van Duyne RP. Detection of a biomarker for Alzheimer's disease from synthetic and clinical samples using a nanoscale optical biosensor. *J. Am. Chem. Soc.* 127(7), 2264–2271 (2005).

60 Riboh JC, Haes AJ, McFarland AD, Yonzon CR, Van Duyne RP. A nanoscale optical biosensor: real-time immunoassay in physiological buffer enabled by improved nanoparticle adhesion. *J. Phys. Chem. B.* 107(8), 1772–1780 (2003).

61 Anker JN, Hall WP, Lyandres O *et al.* Biosensing with plasmonic nanosensors. *Nat. Mater.* 7(6), 442–453 (2008).

62 Sherry LJ, Jin RC, Mirkin CA, Schatz GC, Van Duyne RP. Localized surface plasmon resonance spectroscopy of single silver triangular nanoprisms. *Nano Lett.* 6(9), 2060–2065 (2006).

63 Lu XM, Rycenga M, Skrabalak SE, Wiley B, Xia YN. Chemical synthesis of novel plasmonic nanoparticles. *Ann. Rev. Phys. Chem.* 60, 167–192 (2009).

64 Zoric I, Zach M, Kasemo B, Langhammer C. Gold, platinum, and aluminum nanodisk plasmons: material independence, subradiance, and damping mechanisms. *ACS Nano* 5(4), 2535–2546 (2011).

65 Chan GH, Zhao J, Schatz GC, Van Duyne RP. Localized surface plasmon resonance spectroscopy of triangular aluminum nanoparticles. *J. Phys. Chem. C.* 112(36), 13958–13963 (2008).

66 Alvarez MM, Khoury JT, Schaaff TG *et al.* Optical absorption spectra of nanocrystal gold molecules. *J. Phys. Chem. B.* 101(19), 3706–3712 (1997).

67 Jain PK, El-Sayed MA. Plasmonic coupling in noble metal nanostructures. *Chem. Phys. Lett.* 487(4–6), 153–164 (2010).

68 Chen HJ, Kou XS, Yang Z, Ni WH, Wang JF. Shape- and size-dependent refractive index sensitivity of gold nanoparticles. *Langmuir* 24(10), 5233–5237 (2008).

69 Weissleder R. A clearer vision for *in vivo* imaging. *Nat. Biotechnol.* 19(4), 316–317 (2001).

70 Link S, El-Sayed MA. Size and temperature dependence of the plasmon absorption of colloidal gold nanoparticles. *J. Phys. Chem. B.* 103(21), 4212–4217 (1999).

71 Jain PK, Lee KS, El-Sayed IH, El-Sayed MA. Calculated absorption and scattering properties of gold nanoparticles of different size, shape, and composition: applications in biological imaging and biomedicine. *J. Phys. Chem. B.* 110(14), 7238–7248 (2006).

72 Munechika K, Smith JM, Chen Y, Ginger DS. Plasmon line widths of single silver nanoprisms as a function of particle size and plasmon peak position. *J. Phys. Chem. C.* 111(51), 18906–18911 (2007).

73 Lee KS, El-Sayed MA. Gold and silver nanoparticles in sensing and imaging: Sensitivity of plasmon response to size, shape, and metal composition. *J. Phys. Chem. B.* 110(39), 19220–19225 (2006).

74 Mock JJ, Smith DR, Schultz S. Local refractive index dependence of plasmon resonance spectra from individual nanoparticles. *Nano Lett.* 3(4), 485–491 (2003).

75 Sherry LJ, Chang SH, Schatz GC *et al.* Localized surface plasmon resonance spectroscopy of single silver nanocubes. *Nano Lett.* 5(10), 2034–2038 (2005).

76 Amin RM, Mohamed MB, Ramadan MA, Verwanger T, Krammer B. Rapid and sensitive microplate assay for screening the effect of silver and gold nanoparticles on bacteria. *Nanomedicine (Lond.)* 4(6), 637–643 (2009).

77 Bar-Ilan O, Albrecht RM, Fako VE, Furgeson DY. Toxicity assessments of multisized gold and silver nanoparticles in zebrafish embryos. *Small* 5(16), 1897–1910 (2009).

78 Nehl CL, Liao HW, Hafner JH. Optical properties of star-shaped gold nanoparticles. *Nano Lett.* 6(4), 683–688 (2006).

79 Carbo-Argibay E, Rodriguez-Gonzalez B, Pacifico J *et al.* Chemical sharpening of gold nanorods: the rod-to-octahedron transition. *Angew. Chem. Int. Ed.* 46(47), 8983–8987 (2007).

80 Ma YY, Zeng J, Li WY *et al.* Seed-mediated synthesis of truncated gold decahedrons with a AuCl/Oleylamine complex as precursor. *Adv. Mater.* 22(17), 1930–1934 (2010).

81 Kang T, Hong S, Choi I *et al.* Reversible pH-driven conformational switching of tethered superoxide dismutase with gold nanoparticle enhanced surface plasmon resonance spectroscopy. *J. Am. Chem. Soc.* 128(39), 12870–12878 (2006).

82 Chah S, Kumar CV, Hammond MR, Zare RN. Denaturation and renaturation of self-assembled yeast iso-1-cytochrome c on Au. *Anal. Chem.* 76(7), 2112–2117 (2004).

83 Kim M, Jung SO, Park K *et al.* Detection of Bax protein conformational change using a surface plasmon resonance imaging-based antibody chip. *Biochem. Biophys. Res. Comm.* 338(4), 1834–1838 (2005).

84 Linse S, Helmersson A, Forsen S. Calcium-binding to calmodulin and its globular domains. *J. Biol. Chem.* 266(13), 8050–8054 (1991).

85 Requena J, Whittembury J, Tiffert T, Eisner DA, Mullins LJ. A comparison of measurements of intracellular Ca by Ca electrode and optical indicators. *Biochim. Biophys. Acta.* 805(4), 393–404 (1984).

86 Rich RL, Day YSN, Morton TA, Myszka DG. High-resolution and high-throughput protocols for measuring drug/human serum albumin interactions using BIACORE. *Anal. Biochem.* 296(2), 197–207 (2001).

87 Pockrand I, Swalen JD, Gordon JG, Philpott MR. Surface-plasmon spectroscopy of organic monolayer assemblies. *Surf. Sci.* 74(1), 237–244 (1978).

88 Haes AJ, Zou SL, Zhao J, Schatz GC, Van Duyne RP. Localized surface plasmon resonance spectroscopy near molecular resonances. *J. Am. Chem. Soc.* 128(33), 10905–10914 (2006).

89 Zhao J, Jensen L, Sung JH *et al.* Interaction of plasmon and molecular resonances for rhodamine 6G adsorbed on silver nanoparticles. *J. Am. Chem. Soc.* 129(24), 7647–7656 (2007).

90 Zhao J, Das A, Schatz GC, Sligar SG, Van Duyne RP. Resonance localized surface plasmon spectroscopy: sensing substrate and inhibitor binding to cytochrome P450. *J. Phys. Chem. C.* 112(34), 13084–13088 (2008).

91 Cytochrome P450: *Structure, Function, and Mechanism (3rd Edition).* Kluwer Academic/Plenum, NY, USA, 247–322 (2005).

92 Denisov IG, Makris TM, Sligar SG, Schlichting I. Structure and chemistry of cytochrome P450. *Chem. Rev.* 105(6), 2253–2277 (2005).

93 Dawson JH, Andersson LA, Sono M. Spectroscopic investigations of ferric cytochrome P-450-Cam ligand complexes – identification of the ligand trans to cysteinate in the native enzyme. *J. Biol. Chem.* 257(7), 3606–3617 (1982).

94 Sligar SG. Coupling of spin, substrate, and redox equilibria in cytochrome P450. *Biochemistry (Mosc.)* 15(24), 5399–5406 (1976).

95 Das A, Zhao J, Schatz GC, Sligar SG, Van Duyne RP. Screening of type I and II drug binding to human cytochrome P450–3A4 in nanodiscs by localized surface plasmon resonance spectroscopy. *Anal. Chem.* 81(10), 3754–3759 (2009).

▪ **Notoriously unstable *in vitro*, human cytochrome P450 was bound to a nanoparticle surface and the binding of two types of drugs was monitored with LSPR.**

96 Haes AJ, Hall WP, Chang L, Klein WL, Van Duyne RP. A localized surface plasmon resonance biosensor: first steps toward an assay for Alzheimer's disease. *Nano Lett.* 4(6), 1029–1034 (2004).

97 Anker JN, Hall WP, Lambert MP *et al.* Detection and identification of bioanalytes with high resolution LSPR spectroscopy and MALDI mass spectrometry. *J. Phys. Chem. C.* 113(15), 5891–5894 (2009).

▪ **MALDI MS was combined with LSPR in order to identify bound analytes to a nanoparticle surface.**

98 Lal S, Link S, Halas NJ. Nano-optics from sensing to waveguiding. *Nat. Photonics* 1(11), 641–648 (2007).

▪ **Review of the relationship between the physical features of a given nanoparticle and its plasmon resonance.**

99 Rosi NL, Mirkin CA. Nanostructures in biodiagnostics. *Chem. Rev.* 105(4), 1547–1562 (2005).

100 Schultz S, Smith DR, Mock JJ, Schultz DA. Single-target molecule detection with nonbleaching multicolor optical immunolabels. *Proc. Natl Acad. Sci. USA* 97(3), 996–1001 (2000).

101 Raschke G, Kowarik S, Franzl T *et al.* Biomolecular recognition based on single gold nanoparticle light scattering. *Nano Lett.* 3(7), 935–938 (2003).

102 Chen S, Svedendahl M, Van Duyne RP, Kall M. Plasmon-enhanced colorimetric ELISA with single molecule sensitivity. *Nano Lett.* 11(4), 1826–1830 (2011).

103 Saxton MJ, Jacobson K. Single-particle tracking: applications to membrane dynamics. *Ann. Rev. Biophys. Biomol. Struct.* 26, 373–399 (1997).

104 Baciu CL, Becker J, Janshoff A, Sonnichsen C. Protein-membrane interaction probed by single plasmonic nanoparticles. *Nano Lett.* 8(6), 1724–1728 (2008).

105 Aaron J, Travis K, Harrison N, Sokolov K. Dynamic imaging of molecular assemblies in live cells based on nanoparticle plasmon resonance coupling. *Nano Lett.* 9(10), 3612–3618 (2009).

106 Hong QA, Sheetz MP, Elson EL. Single-particle tracking – analysis of diffusion and flow in 2-dimensional systems. *Biophys. J.* 60(4), 910–921 (1991).

107 Xu XHN, Chen J, Jeffers RB, Kyriacou S. Direct measurement of sizes and dynamics of single living membrane transporters using nanooptics. *Nano Lett.* 2(3), 175–182 (2002).

108 Bingham JM, Willets KA, Shah NC, Andrews DQ, Van Duyne RP. Localized surface plasmon resonance imaging: simultaneous single nanoparticle spectroscopy and diffusional dynamics. *J. Phys. Chem. C.* 113(39), 16839–16842 (2009).

▪▪ **Individual moving nanoparticles were tracked in real time and, simultaneously, their LSPR spectra were collected.**

109 Jin RC, Cao YW, Mirkin CA *et al.* Photoinduced conversion of silver nanospheres to nanoprisms. *Science* 294(5548), 1901–1903 (2001).

110 Taton TA, Lu G, Mirkin CA. Two-color labeling of oligonucleotide arrays via size-selective scattering of nanoparticle probes. *J. Am. Chem. Soc.* 123(21), 5164–5165 (2001).

111 El-Sayed IH, Huang XH, El-Sayed MA. Surface plasmon resonance scattering and absorption of anti-EGFR antibody conjugated gold nanoparticles in cancer diagnostics: applications in oral cancer. *Nano Lett.* 5(5), 829–834 (2005).

112 Alivisatos P. The use of nanocrystals in biological detection. *Nat. Biotechnol.* 22(1), 47–52 (2004).

113 Hu R, Yong KT, Roy I *et al.* Metallic nanostructures as localized plasmon resonance enhanced scattering probes for multiplex dark-field targeted imaging of cancer cells. *J. Phys. Chem. C.* 113(7), 2676–2684 (2009).

114 Huang XH, Jain PK, El-Sayed IH, El-Sayed MA. Plasmonic photothermal therapy (PPTT) using gold nanoparticles. *Laser Med. Sci.* 23(3), 217–228 (2008).

▪ **Review on the latest plasmonic nanoparticle-based biological imaging and photothermal therapy.**

115 Loo C, Lowery A, Halas NJ, West J, Drezek R. Immunotargeted nanoshells for integrated cancer imaging and therapy. *Nano Lett.* 5(4), 709–711 (2005).

116 Kumar S, Harrison N, Richards-Kortum R, Sokolov K. Plasmonic nanosensors for imaging intracellular biomarkers in live cells. *Nano Lett.* 7(5), 1338–1343 (2007).

117 Fong WK, Hanley TL, Thierry B, Kirby N, Boyd BJ. Plasmonic nanorods provide reversible control over nanostructure of self-assembled drug delivery materials. *Langmuir* 26(9), 6136–6139 (2010).

118 Tam JM, Tam JO, Murthy A *et al.* Controlled assembly of biodegradable plasmonic nanoclusters for near-infrared imaging and therapeutic applications. *ACS Nano* 4(4), 2178–2184 (2010).

119 Rosi NL, Giljohann DA, Thaxton CS *et al.* Oligonucleotide-modified gold nanoparticles for intracellular gene regulation. *Science* 312(5776), 1027–1030 (2006).

120 Wustholz KL, Henry AI, McMahon JM *et al.* Structure-activity relationships in gold nanoparticle dimers and trimers for surface-enhanced Raman spectroscopy. *J. Am. Chem. Soc.* 132(31), 10903–10910 (2010).

121 Lyandres O, Yuen JM, Shah NC *et al.* Progress toward an *in vivo* surface-enhanced Raman spectroscopy glucose sensor. *Diabet. Technol. Ther.* 10(4), 257–265 (2008).